INTERNATIONAL JOURNAL OF PRECISION ENGINEERING AND MANUFACTURING Vol. 17, No. 12, pp. 1659-1664 DECEMBER 2016 / 1659
DOI: 10.1007/s12541-016-0192-8 ISSN 2234-7593 (Print) / ISSN 2005-4602 (Online)

Microstructure, Mechanical Properties and Failure Mechanisms of Resistance Spot Welding Joints between Ultra High Strength Steel 22MnB5 and Galvanized Steel HSLA350

Xuebo Liang[1], Xinjian Yuan[1,#], Haodong Wang[1], Xiuyang Li[1], Ci Li[1], and Xueyu Pan[2]

1 College of Materials Science and Engineering, Chongqing University, No. 174, Shazhengjie Street, Shapingba District, Chongqing, 400045, China
2 Body Shop, Plant 2, Changan Ford Automobile Co., Ltd., No. 666, Jinshan Road, New Northern Zone, Chongqing, 401122, China
Corresponding Author / E-mail: xinjianyuan@yahoo.com, TEL: +86-13618255866

KEYWORDS: Ultra high strength steel, Resistance spot welding, Microstructure, Mechanical property, Fracture mechanism

Resistance spot welding of 22MnB5/HSLA350 and its weldability are investigated. From base material to the nugget, the microstructure of 22MnB5 side can be expressed as M/tempered M+ granular carbides/F+M/fine M/lath M, and on HSLA350 side, F+M/F+flocculent P+tempered M/F+flocculent P+M/F+M/lath M are observed. The heat-affected zone (HAZ) of 22MnB5 exhibits obvious softening region and strengthening region caused by the tempered M and quite fine M, respectively. The peak load of welded joints undergoes two stages of a dramatic increase and a subsequent decrease with increases in the welding current. The maximum value (13.82 kN) of peak load is achieved at a welding current of 8 kA. The failure modes involving interfacial failure (IF), pullout failure from the galvanized steel (PFG), pullout failure from boron steel and tearing of the galvanized steel (PFB-TG) and pullout failure from the boron steel (PFB) are discussed in detail.

Manuscript received: February 3, 2016 / Revised: March 15, 2016 / Accepted: July 29, 2016

1. Introduction

With the steady rising for vehicle safety, fuel efficiency and light weight, ultra-high strength steels (UHSS) are increasingly applied in automotive bodies. Hot stamping boron steels with a fully martensitic microstructure and a tensile strength over 1500 MPa have been becoming one of the most promising materials in car anti-collision structure parts, like front and rear bumper beams, A-pillars, B-pillars, roof rails, side rails, tunnels, and reinforced sheet of door.[1,2]

Resistance spot welding (RSW) procedure, a welding method of heat source stem from the resistant heat generated at the contact interface and adjacent region of metals, is an important joining technology in body-in-white manufacture. Goodarzi et al. studied the microstructure and failure behavior of the galvanized low carbon steels joints produced by RSW and concluded that weld nugget is mainly composed of martensite (M) resulted from high cooling rate.[3] Yu developed a predictive model using a logistic regression model to analyze the effects of welding variables on welding quality.[4]

Mechanical properties and fracture modes of 22MnMoB hot-stamping quenched boron steel welded joints mainly depend on nugget diameter. Jong et al. found that the HAZ of typical Al-Si-coated USIBOR 1500 welded joint utilizing RSW could be divided into three areas: tempered zone, fine grain zone and coarse grain zone, and an obvious softening behavior in tempered zone with the microstructure of ferrite (F) and tempered M was observed.[5]

The ultra high strength (e.g., the hot stamping boron steel 22MnB5) components are usually assembled with other automotive plates (e.g., the galvanized steel HSLA350) by RSW. The above two metals have different chemical composition, microstructure, coating layers, mechanical properties and physical properties, thus, the HAZ size, indentation rate and fracture modes of their RSW joints are dramatically different from those of the joints of similar steels. However, there are few literatures about the RSW between hot stamping boron steel and galvanized low carbon steel.

The main objective of present study is to investigate and characterize the microstructure, mechanical properties and the fracture modes of

Table 1 Chemical composition of 22MnB5 and HSLA350

Steel	Chemical composition (wt.%)					
	C	Mn	Si	Cr	B	Fe
22MnB5	0.23	1.5	0.45	0.16	0.002	Bal.
HSLA350	0.05	0.62	0.05	0.04	-	Bal.

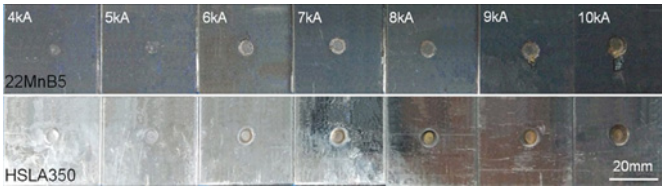

Fig. 1 Macro photographs of welded spots with different currents

RSW joints between 22MnB5 and HSLA350 steels. The microstructural features with particular emphasis on HAZ were analyzed using scanning electron microscopy (SEM) and transmission electron microscopy (TEM). An in-depth examination on the relationship between microstructure and tensile-shear strength was performed, and the mechanisms governing the fracture were also interpreted in detail.

2. Experimental Procedure

Medium frequency direct current welding machine (OBARA, SIV21) was used to conduct RSW experiments. The electrodes with a conical tip of 6 mm in diameter were made from RWMA class II Copper-chromium material. The 1.35 mm thick hot stamping boron steel (Al-Si coated layer with 45 μm) and 1.5 mm thick galvanized steel HSLA350 (Zn layer with 15 μm) were applied as the base metals (BMs). The chemical composition of BMs is given in Table 1.

A series of welding currents were selected for RSW experiments at an electrode force of 3.2 kN and a welding time of 12 cycles. For metallographic examinations, the welded joints were cut using an electrical discharge cutting machine, grounded with SiC papers, polished on 0.03 mm alumina and etched by a 4% nital solution for 7-12 s at room temperature. The cross-sectional microstructure and fracture surface of the joints were characterized using optical microscope (OM) and scanning electron microscope (SEM), and the microstructure of fusion zone (FZ) was also identified by transmission electron microscope (TEM). The micro-Vickers hardness measurement on cross section of welded joints was conducted with a load of 500 g and a dwelling time of 10 s, and the indentations were spaced 0.15 mm apart. Tensile-shear tests were performed using a tensile testing machine with 2 mm/min tensile velocity in room temperature. The fracture mechanisms were also analyzed by OM and SEM.

3. Results and Discussion

3.1 Macro characteristics of welded joints

Generally, the quality and strength of a RSW joint can be judged by nugget diameter and indentation rate.[3] In order to obtain a qualified

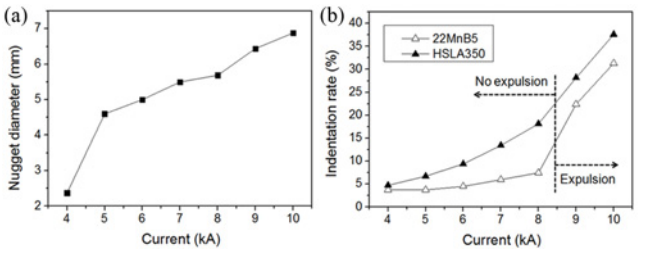

Fig. 2 Macro characteristics of joints according to the welding current: (a) nugget diameter and (b) indentation rate

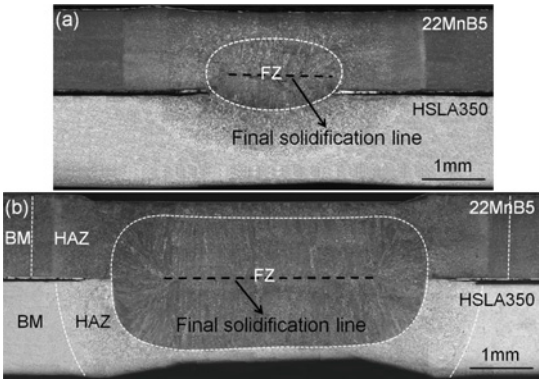

Fig. 3 Typical macrostructure of the joints welded with the welding currents (a) 4 kA and (b) 8 kA

welding joint, the indentation rate should be less than 20% of steel thickness.[6] Macro photographs of the joints welded with different current, ranging from 4 kA to 10 kA are shown in Fig. 1. When the welding current is lower or equal to 8 kA, the surfaces of welded joints are clean. With the increasing of welding current, burrs caused by expulsion appear on the surface of welded joints. The effect of welding current on the nugget diameter of welded joints is illustrated in Fig. 2(a). Increasing welding current leads to the high heat input, and thus the nugget diameter increases.

As shown in Fig. 2(b), the indentation rate also demonstrates an increasing trend with the increase of welding current, varying from 4 kA to 10 kA. The indentation rate of HSLA350 side is always higer than that of the 22MnB5 side. When the current is greater than or equal to 7 kA, on the HSLA350 steel side, the surfaces of welded joints began to appear obvious indentation as shown in Fig. 1. The result is mainly due to lower hardness of HSLA350. When the welding current is greater than 8 kA, the indentation rate exceeds 20%, since welding spots experience an expulsion. Expulsion causes an excessive indentation, and such indentation results in significant material flow and gross deformation within the sheet metal.[7]

3.2 Microstructure of welded joints

Fig. 3 demonstrates typical macrostructure of joints prepared with 4 kA and 8 kA, when welding time is 12 cycles and electrode force is 3.2 kN. The final solidification line, indicated with dashed lines in Fig. 3, is located on the geometrical center of FZ, rather than the sheet/sheet interface, as reported earlier.[8] It is well-known that the 22MnB5 steel

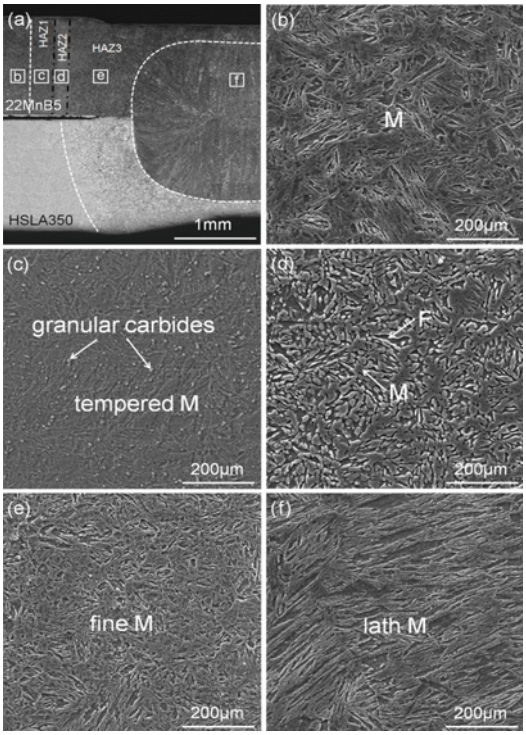

Fig. 4 Microstructural characteristics of welded spot on the 22MnB5 side: (a) overall view of the sample where the location of micrographs, (b) base metal (BM), (c) heat affected zone 1 (HAZ1), (d) heat affected zone 2 (HAZ2), (e) heat affected zone 3 (HAZ3) and (f) FZ

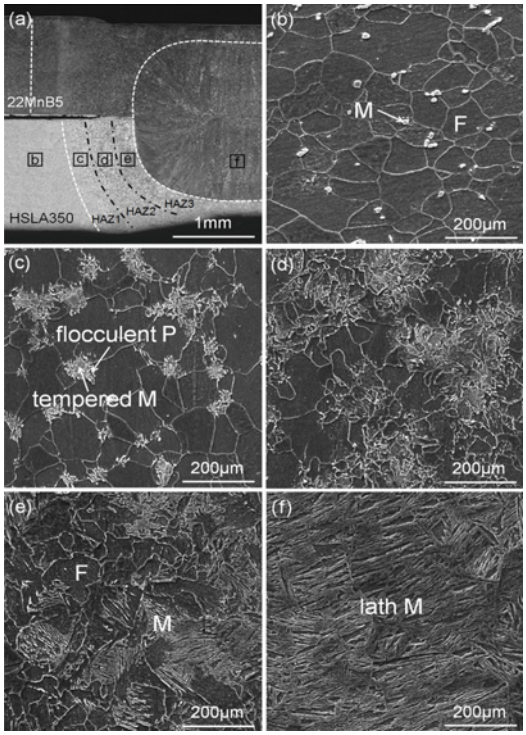

Fig. 5 Microstructural characteristics of welded spot on the HSLA350 side: (a) overall view of the sample where the location of micrographs, (b) BM, (c) HAZ1, (d) HAZ2, (e) HAZ3 and (f) FZ

has greater resistivity than that of HSLA350 steel. Therefore, when the nugget is relatively small, most of FZ is located on the side of 22MnB5, as shown in Fig. 3(a). The good joint without the weld defect cracks, pores, and shrinkage porosities is obtained under the welding current of 8 kA (Fig. 3(b)). The joint can be divided into three zones: BM, HAZ and FZ, and the boundaries between two adjacent zones are clearly depicted with white dashed lines in Fig. 3(b).

The microstructural characteristics of different zones in the welding region were analyzed with SEM and TEM, and the results are given in Figs. 4-5 and Fig. 6, respectively. Fig. 4(b) presents that the BM of 22MnB5 steel is full martensite and a small amount of martensite dispersed at the grain boundaries of ferrite matrix is observed in the BM of HSLA350 as shown in Fig. 5(b) SEM images of HAZ are given in Fig. 4(c)-(e) and Fig. 5(c)-(e). As presented in Fig. 4(a) and Fig. 5(a), the HAZ can be divided into three parts: HAZ1, HAZ2 and HAZ3, with respect to different microstructure. For 22MnB5, the microstructure of HAZ can be expressed as tempered M+granular carbides/F+M/fine M. The HAZ1 is regarded as the zone in immediate vicinity of BM (Fig. 4(c)). In HAZ1, the granular carbides are observed in the tempered martensite matrix and amount of granular carbides increases gradually along the direction from the BM to FZ. Because peak temperature of HAZ1 is lower than the austenitizing temperature, the pre-existing martensite is tempered and then the granular carbides are precipitated. A double phase, ferrite and martensite, is noted in HAZ2 (Fig. 4(d)). On one hand, the microstructure undergoes an incomplete austenitic transformation during the welding process while on the other hand, cooling rate in the HAZ2 is lower than FZ, thus a part of austenite

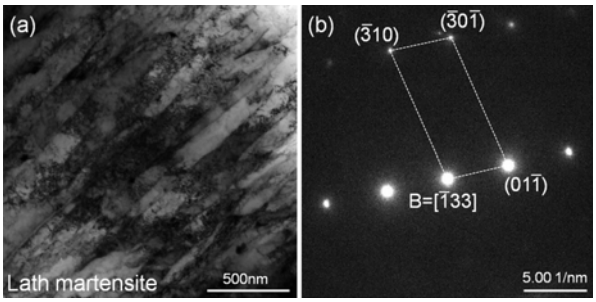

Fig. 6 TEM analysis of the FZ: (a) TEM micrograph and (b) diffraction pattern

transform into ferrite during cooling. The HAZ3 consists of quite fine martensite as shown in Fig. 4(e). The prior martensite experiences a complete austenitic transformation, and austenite grains only have a very short time to coarsen, and then the fine martensite is transformed from austenite due to rapid cooling rate during RSW.[9] In case of HSLA 350, the HAZ microstructure can be expressed as F+flocculent pearlite (P)+tempered M/F+flocculent P+M/F+M from BM side to the FZ side. A small amount of flocculent pearlite generates around the tempered martensite in the HAZ1 (Fig. 5(b)). In HAZ1, the peak temperature is below austenitizing temperature, therefore, the carbon precipitates from saturated martensite in the tempering procedure and carbides form. The carbides combine with the ferrite of the BM, and the flocculent pearlite appears. In HAZ2, the peak temperature is slightly higher than the austenitic temperature during RSW, so the zone experiences an

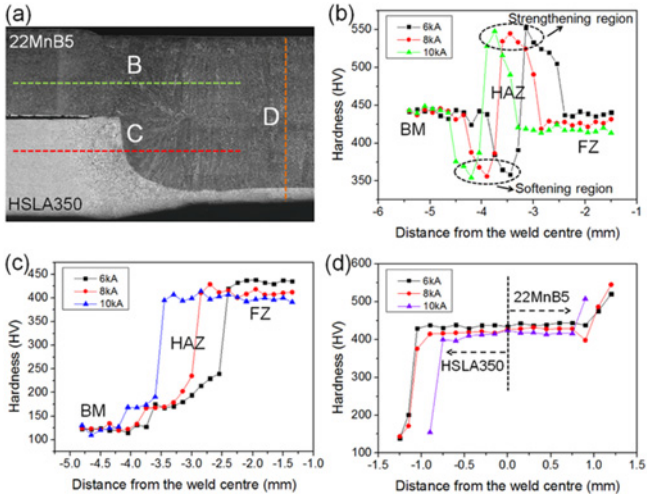

Fig. 7 Hardness profiles of joints with 6 kA, 8 kA and 10 kA: (a) overall view of the sample where the location of micro-hardness traverse, (b) 22MnB5 side, (c) HSLA350 side and (d) the center region of nugget along the direction perpendicular to the plate surface

incomplete austenitic transformation. The respective proportion of martensite and pearlite in the HAZ2 is larger compared with HAZ1. The HAZ3 undergoes a temperature well above the austenitic temperature during RSW, which makes the pre-existing martensite experiences a complete austenitic transformation. Since cooling rate of this zone is below the FZ, the microstructure includes ferrite and martensite, as shown in Fig. 5(d).

In FZ, the temperature is beyond the liquidus during RSW. So, in this area, both of the steels show lath martensite (Fig. 4(e), 5(e) and 6). The grains tend to grow in vertical direction of solid/liquid interface and show columnar structure, which is mainly dominated by the high temperature gradient during solidification.[10]

3.3 Micro-hardness of welded joint

Fig. 7 shows micro-hardness values of three different welded joints obtained in different currents of 6 kA, 8 kA and 10 kA, respectively.

On the 22MnB5 side (Fig. 7(b)), both the BM and FZ exhibit high hardness values owing to the present martensite. The hardness in BM is slightly higher compared with FZ due to smaller grain size in FZ compared to BM. It is noteworthy that the hardness of FZ is higher at welding current of 6 kA. The FZ is mainly composed of the martensite phase, so the hardness is determined by carbon content. The FZ of joint welded under 6 kA has relatively higher carbon contents in virtue of the final solidification line of the nugget locating on 22MnB5 side. A significant decrease in the hardness to about 360 HV obviously appears in the HAZ (Fig. 7(b)), compared with the hardness of the BM and FZ. The matensite of 22MnB5 after RSW transforms to soft tempered martensite and ferrite due to weld thermal cycle effect. Jong et al. reported the hardness of the fine grain HAZ (near FZ) is similar to FZ.[5] But, in this study, the highest hardness of about 540 HV is observed in HAZ close to FZ. According to the analysis of microstructure, it is thought that the quite fine martensite contributes to the highest hardness.

As shown in Fig. 7(c), the hardness of the FZ is significantly higher

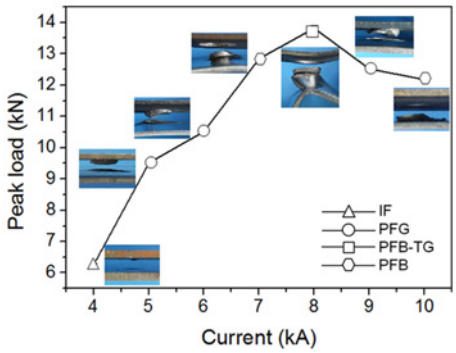

Fig. 8 Peak load of welded spot versus the welding current

than that of the BM, owing to the significantly higher percentage of martensite in FZ contrast with BM. Similar to the 22MnB5, there is a slight change in the hardness of FZ at different welding current.

The hardness of HAZ increases gradually, which is caused by the formation of more martensite with the increase of peak temperature during RSW. The hardness profile in central region of nugget along the direction perpendicular to the plate surface is presented in Fig. 7(d). The same hardness of two materials in FZ conveys that the composition of FZ is more or less uniformly distributed. Areas near the surfaces of plates and contact with electrodes during RSW. The hardness value of 22MnB5 side increases, while hardness value of HSLA350 side decreases. It is noticeable that there is no softening region in 22MnB5 side due to high cooling rate and high electrode pressure.

3.4 Mechanical properties and fracture modes

In the tensile-shear tests, the peak load and fracture modes of welded spots, gained with a serial of weld currents 4, 5, 6, 7, 8, 9 and 10 kA, are summarized in Fig. 8.

With increasing of welding current from 4 kA to 8 kA, the peak load of welded joints is enhanced from 6.24 kN to 13.82 kN. When welding current is larger than 8 kA, peak load reduces gradually with the increasing of welding current. Wei et al. found that the change trends of failure load and nugget diameter are similar with welding current, and then they inferred that the change of failure load mainly depends on the nugget diameter.[9] However, in this study, the peak load does not increase monotonically as the nugget diameter largened (Fig. 8 and 2(a)). When current exceeds 8 kA, the expulsion during RSW causes excessive indentation rate and excessive thin joint, and thus the resultant joint has a reduction of load-carrying capability. It can be concluded that the welding current mainly alters the nugget diameter and the indentation rate and then affects the mechanical properties of welded joint.

In general, the single-spot welding of different materials often exhibits two different fracture modes (interfacial failure (IF) and pullout failure (PF)) in tensile-shear tests. Choi et al. observed that only IF mode in tensile-shear testing for RSW of GA780DP and hot-stamped 22MnB5 steel sheets, and high load-carrying capacity is obtained in this failure mode.[11]

However, as shown in Figs. 8 and 9, there are four different failure modes, which are termed as: the interfacial failure (IF), the pullout failure from the galvanized steel (PFG), the pullout failure on boron steel and tearing the galvanized steel (PFB-TG) and the pullout failure

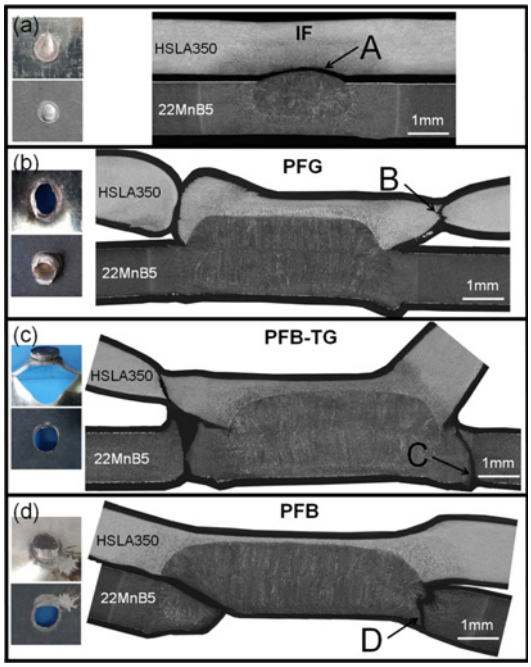

Fig. 9 Typical images and the macrostructures of the four failure joints: (a) IF mode, (b) PFG mode, (c) PFB-TG mode and (d) PFB mode

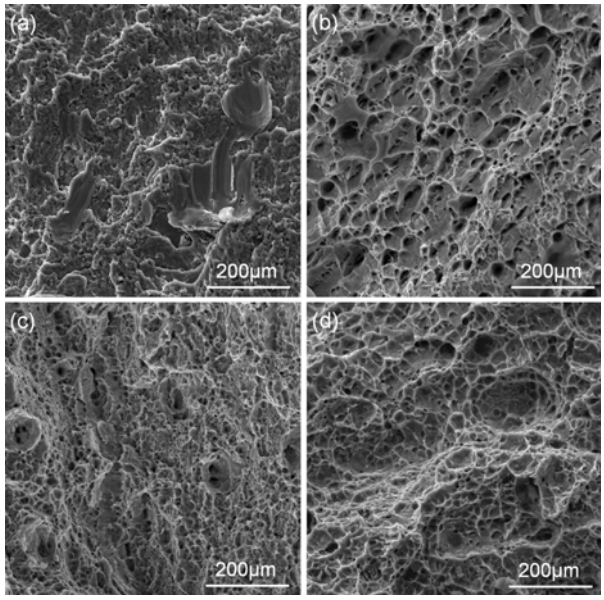

Fig. 10 Typical SEM micrographs of different fracture surfaces taken from Fig. 9: (a) location 'A' in Fig. 9(a), (b) location 'B' in Fig. 9(b), (c) location 'C' in Fig. 9(c) and (d) location 'D' in Fig. 9(d)

from the boron steel (PFB). Fig. 8 presents the changes in the failure modes of the 22MnB5 /HSLA350 RSW joints in different welding current. The cross section morphology of IF mode is shown in Fig. 9(a). It is thought that the nugget is too small that it can not to resist the stress concentration at the circumference of nugget during tensile-shear testing.[12] For PFG mode (Fig. 9(b)), when the nugget is big enough to resist IF mode, HSLA350 sheet close to the nugget will take place obvious plastic deformation and cause a rotation in stretch direction. The crack occurs at the boundary of BM and HAZ, as a result of necking and stress concentration derived from the different ductility between BM and HAZ. The most appropriate nugget diameter and indentation rate of welded joint can carry the maximum tensile-shear load and lead to a PFB-TG mode (Fig. 9(c)). As the tensile-shear load increased, the necking and crack emergence at the boundary of BM and HAZ of the HSLA350 steel. The larger nugget has longer boundary to resist the stress concentration so that the crack extends to BM and the HSLA350 develop a lager rotation as the proceeding of tensile-shear loading. The more rotation the larger pull-out load on the welded joint of 22MnB5 side, and thus fracture occurs in the softening region of welded joint of 22MnB5 side. The typical PFB mode is shown in Fig. 9(d). The pullout failure initiates from 22MnB5 side, and a simultaneous slight necking and rotation appears in HSLA350. The excessive indentation rate resulting from enormous expulsion raises the sharp stress concentration at the boundary of indentation, which decreases pull-out load-carrying capacity of welded joint. The crack initiates at the boundary of indentation in the thinner 22MnB5, and propagates perpendicular to the plate surface under pull-out loading.

It can be seen from the typical SEM micrographs of the fracture surfaces (Fig. 10), the fractography of welded spot (Fig. 10(a)) conveys IF mode involved a brittle pattern, which may result from the weld defect crack, shrinkage porosity and pore. But, the dimple base fracture feature is observed for PFG, PFB-TG and PFB failure modes. Generally, the plasticity of material dominates the size and depth of dimples and plastic deformation before fracture of the HSLA350 is significantly larger than that of 22MnB5, so the bigger and deeper dimples are presented in the fracture surface of the HSLA350 (Fig. 10(b)) than that of the 22MnB5 (Figs. 10(c) and 10(d)).

4. Conclusions

Microstructure, mechanical properties and fracture modes of RSW dissimilar 22MnB5/HSLA350 weld joints are discussed in detail, leading to the following conclusions:

1. Under the welding current of 4 kA, most of the FZ of welded joint is located on the side of 22MnB5. The sound joint without the weld defect cracks, pores, and shrinkage porosities etc. is obtained at 8 kA. The welded spot can be divided into three zones: BM, HAZ and FZ. In 22MnB5, the HAZ exhibits obvious softening region and strengthening region, which can be explained by their different microstructures: tempered M+granular carbides and fine M. For HSLA 350, the hardness values of HAZ increases gradually from BM to FZ. The FZ consists of full lath martensite. In contrast with 8 kA and 10 kA, a higher hardness value of the FZ is obtained in 6 kA, which is attributed to the higher carbon contents.

2. With the raising of heat input, nugget diameter and indentation rate increase gradually. In tensile-shear tests, largest peak load (13.82 kN) of the joint is obtained at 8 kA. When the welding current is larger than 8 kA, the excessive indentation resulting from the present expulsion may responsible for the reduction of the peak load.

3. From the tensile-shear testing, the IF, PFG, PFB-TG and PFB modes appear in 22MnB5/HSLA350 RSW joints. The four failure modes

have a strong correlation with the microstructure, nugget diameter and indentation rate of the welded joints. The fracture morphology indicates that IF mode includes a brittle pattern. The fracture surfaces for PFG, PFB-TG and PFB modes exhibit a lot of dimples. The dimples in the fracture surface of the HSLA350 are bigger and deeper than that of the 22MnB5, as the result of large plasticity of HSLA350.

ACKNOWLEDGEMENT

The authors would like to express their thanks to Dr. Yanyan Huang for the helpful discussions. The authors gratefully acknowledge the financial support provided by National Natural Science Foundation of China (No. 51205428).

REFERENCES

1. Liang, W., Liu, Y., Zhu, B., Zhou, M., and Zhang, Y., "Conduction Heating of Boron Alloyed Steel in Application for Hot Stamping," Int. J. Precis. Eng. Manuf., Vol. 16, No. 9, pp. 1983-1992, 2015.
2. Jiang, C., Shan, Z., Zhuang, B., Zhang, M., and Xu, Y., "Hot Stamping Die Design for Vehicle Door Beams using Ultra-High Strength Steel," Int. J. Precis. Eng. Manuf., Vol. 13, No. 7, pp. 1101-1106, 2012.
3. Goodarzi, M., Marashi, S., and Pouranvari, M., "Dependence of Overload Performance on Weld Attributes for Resistance Spot Welded Galvanized Low Carbon Steel," Journal of Materials Processing Technology, Vol. 209, No. 9, pp. 4379-4384, 2009.
4. Yu, J., "Quality Estimation of Resistance Spot Weld based on Logistic Regression Analysis of Welding Power Signal," Int. J. Precis. Eng. Manuf., Vol. 16, No. 13, pp. 2655-2663, 2015.
5. Jong, Y.-S., Lee, Y.-K., Kim, D.-C., Kang, M.-J., Hwang, I.-S., and Lee, W.-B., "Microstructural Evolution and Mechanical Properties of Resistance Spot Welded Ultra High Strength Steel Containing Boron," Materials Transactions, Vol. 52, No. 6, pp. 1330-1333, 2011.
6. Zhang, H., Qiu, X., Bai, Y., Xing, F., Yu, H., and Shi, Y., "Resistance Spot Welding Macro Characteristics of the Dissimilar Thickness Dual Phase Steels," Materials & Design, Vol. 63, pp. 151-158, 2014.
7. Han, Z. and Indacochea, J., "Effects of Expulsion in Spot Welding of Cold Rolled Sheet Steels," Journal of Materials Engineering and Performance, Vol. 2, No. 3, pp. 437-444, 1993.
8. Marashi, S. P. H., Pouranvari, M., Salehi, M., Abedi, A., and Kaviani, S., "Overload Failure Behaviour of Dissimilar Thickness Resistance Spot Welds during Tensile Shear Test," Materials Science and Technology, Vol. 26, No. 10, pp. 1220-1225, 2010.
9. Wei, S. T., Lv, D., Liu, R. D., Lin, L., Xu, R. J., et al., "Similar and Dissimilar Resistance Spot Welding of Advanced High Strength Steels: Welding and Heat Treatment Procedures, Structure and Mechanical Properties," Science and Technology of Welding and Joining, Vol. 19, No. 5, pp. 427-435, 2014.
10. Zhang, H., Wei, A., Qiu, X., and Chen, J., "Microstructure and Mechanical Properties of Resistance Spot Welded Dissimilar Thickness DP780/DP600 Dual-Phase Steel Joints," Materials & Design, Vol. 54, pp. 443-449, 2014.
11. Choi, H.-S., Park, G.-H., Lim, W.-S., and Kim, B.-m., "Evaluation of Weldability for Resistance Spot Welded Single-Lap Joint between GA780DP and Hot-Stamped 22MnB5 Steel Sheets," Journal of Mechanical Science and Technology, Vol. 25, No. 6, pp. 1543-1550, 2011.
12. Pouranvari, M. and Marashi, S., "Failure Mode Transition in AHSS Resistance Spot Welds. Part I. Controlling Factors," Materials Science and Engineering: A, Vol. 528, No. 29, pp. 8337-8343, 2011.